FEATURE ARTICLE

Water Dynamics—The Effects of Ions and Nanoconfinement

Sungnam Park, David E. Moilanen, and M. D. Fayer*

Department of Chemistry Stanford University, Stanford, California 94305

Received: December 31, 2007; In Final Form: February 13, 2008

Hydrogen bond dynamics of water in highly concentrated NaBr salt solutions and reverse micelles are studied using ultrafast 2D-IR vibrational echo spectroscopy and polarization-selective IR pump−probe experiments performed on the OD hydroxyl stretch of dilute HOD in H_2O. The vibrational echo experiments measure spectral diffusion, and the pump−probe experiments measure orientational relaxation. Both experimental observables are directly related to the structural dynamics of water's hydrogen bond network. The measurements performed on NaBr solutions as a function of concentration show that the hydrogen bond dynamics slow as the NaBr concentration increases. The most pronounced change is in the longest time scale dynamics which are related to the global rearrangement of the hydrogen bond structure. Complete hydrogen bond network randomization slows by a factor of ∼3 in ∼6 M NaBr solution compared to that in bulk water. The hydrogen bond dynamics of water in nanoscopically confined environments are studied by encapsulating water molecules in ionic head group (AOT) and nonionic head group (Igepal CO 520**)** reverse micelles. Water dynamics in the nanopools of AOT reverse micelles are studied as a function of size by observing orientational relaxation. Orientational relaxation dynamics deviate significantly from bulk water when the size of the reverse micelles is smaller than several nm and become nonexponential and slower as the size of the reverse micelles decreases. In the smallest reverse micelles, orientational relaxation (hydrogen bond structural randomization) is almost 20 times slower than that in bulk water. To determine if the changes in dynamics from bulk water are caused by the influence of the ionic head groups of AOT or the nanoconfinement, the water dynamics in 4 nm nanopools in AOT reverse micelles (ionic) and Igepal reverse micelles (nonionic) are compared. It is found that the water orientational relaxation in the 4 nm diameter nanopools of the two types of reverse micelles is almost identical, which indicates that confinement by an interface to form a nanoscopic water pool is a primary factor governing the dynamics of nanoscopic water rather than the presence of charged groups at the interface.

I. Introduction

This article draws together a variety of materials,[1−6] which have not been considered jointly, to tell one story. The combined results may say something important about biological systems even though no biological molecules are involved in the studies. The results should also be significant for materials other than biological systems even though such materials are not considered explicitly. The issues to be addressed here are the combined roles of ions and nanoscopic confinement in modifying the dynamical properties of water. How much are the dynamics of water changed when the water molecules are associated with ions? If water is in a confined space of nanometer dimensions or a few nanometers from an interface, does the interface have to be ionic to have a pronounced effect on water hydrogen bond dynamics or is merely being confined by the interface sufficient to strongly influence hydrogen bond network dynamics?

Water is ubiquitous in nature and plays an important role in chemical, physical, and biological processes. In the pure liquid, water molecules are hydrogen bonded to neighboring water molecules in an approximately tetrahedral geometry and form an extended hydrogen bond network. Hydrogen bond lengths (strengths) are continually changing, and water molecules are constantly switching hydrogen bond partners.[7−12] The structure of water fluctuates on femtosecond to picosecond time scales.[7−9,11−13] The slowest component of the fluctuations is associated with the global structural rearrangement of the hydrogen bond network.[9] Rapid structural evolution of the hydrogen bond network of water is responsible for water's unique properties.[14] The properties and dynamics of water are changed in the presence of charges and in nanoscopically confined environments.[1−4,15−28] In aqueous solutions, water dissolves ionic compounds, charged chemical species, and macromolecules with charged surfaces including proteins, micelles, and lipid bilayers by forming hydration shells (layers) around them. In nanoscopic water environments, water molecules are in direct contact with different types of interfaces. At and near an interface, water's hydrogen bond network is significantly modified because the network must make accommodation for the distinct topology of the interface. Water confined on nanometer length scales is found in many physical and biological environments. Near charges or interfaces, the

* To whom correspondence should be addressed. E-mail: fayer@stanford.edu.

10.1021/jp7121856 CCC: $40.75
Published on Web 03/28/2008

Sungnam Park was born in Gangjin, Korea, in 1973. He received his B.A. degree (1997) and M.S. degree (1999) in Chemistry from Korea University. He earned his Ph.D. degree (2005) in Chemistry from the University of Chicago with Professor Norbert F. Scherer. Currently, he is doing post-doctoral research with Professor Michael D. Fayer at Stanford University. His current research interests include development and applications of ultrafast 2D IR spectroscopy.

David E. Moilanen was born in Redmond, Washington in 1980. He received B.S. degrees in Chemistry and Physics from the University of Washington in 2003. Currently, he is a graduate student with Professor Michael D. Fayer at Stanford University. His research focuses on applying ultrafast infrared spectroscopy to study the properties and dynamics of water and aqueous systems.

properties and dynamics of water cannot be extrapolated from those of bulk water and need to be examined.

The hydroxyl (OH and OD) stretch frequency of water in aqueous solutions is closely related to the local hydrogen bond structure. Since the advent of ultrafast femtosecond infrared techniques, time-resolved IR spectroscopies have been applied to study many aqueous systems. IR pump−probe experiments have been used extensively to study vibrational population relaxation[29,30] and orientational relaxation dynamics of pure water,[31−34] water in nanoscopic environments,[4,5,35,36] and ionic solutions.[37−40] Over the last several years, the application of ultrafast infrared vibrational echo spectroscopy,[13,41−47] particularly two-dimensional infrared (2D-IR) vibrational echo experiments,[1,9,48−51] combined with molecular dynamics (MD) simulations[7,52−54] has greatly enhanced the understanding of the hydrogen bond dynamics in pure water.[7−9,11−13,52−54] More recently, 2D-IR vibrational echo spectroscopy was used to study the hydrogen bond dynamics of water in highly concentrated ionic solutions.[1,2]

Here, we present the results of linear and nonlinear IR experiments performed on highly concentrated ionic solutions and reverse micelles to understand the effects of charges and nanoscopic confinements on the properties and dynamics of

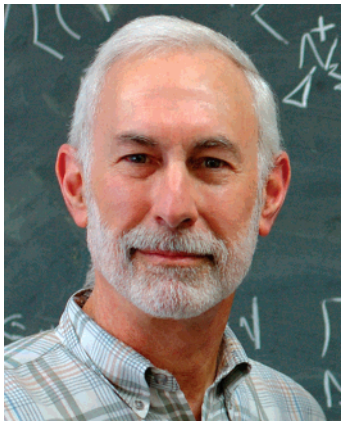

Michael D. Fayer was born in Los Angeles, California in 1947. He received his B.S. and Ph.D. degrees in Chemistry from the University of California at Berkeley in 1969 and 1974, respectively. He is currently the D. M. Ehrsam and E. C. Franklin Professor of Chemistry at Stanford University. He is a member of the National Academy of Sciences and the 2007 recipient of the E. Bright Wilson Award for Spectroscopy presented by the American Chemical Society. Throughout his career, he has been involved in the development and application of ultrafast nonlinear spectroscopic techniques for the study of complex molecular systems.

water. Highly concentrated NaBr solutions are investigated to study the dynamics of water in close proximity to ions. The number of water molecules per NaBr ranges from 8 to 32. These numbers of water molecules would correspond to less than one hydration shell to approximately two hydration shells for each ion in dilute solution. By examining such highly concentrated NaBr solutions, all of the water molecules are close to ions, and therefore, the influence of water−ion interactions is not diluted out by large quantities of bulk water unaffected by ions. Using both ultrafast 2D-IR vibrational echo experiments and polarization-selective pump−probe experiments, it is shown that the dynamics of water in concentrated salt solutions differ significantly from those of pure water, but not to the extent indicated earlier by less direct measurements.[37] The surprising result is that even at the highest concentration with 8 water molecules per NaBr (~6 M solution), the time scale associated with the complete rearrangement of the hydrogen bond structure is only a factor of 3 slower than that in pure water.

To examine the influence of nanoconfinement on water dynamics, reverse micelles are used. Reverse micelles are surfactant assemblies that encapsulate nanoscopic pools of water. For some well-characterized reverse micelles, the size of the water pool is readily controlled on nanometer length scales by changing the concentration ratio of water and surfactant, $w_0 = [H_2O]/[\text{surfactant}]$. The diameter of spherical reverse micelles depends linearly on the w_0 parameter over a range of sizes. A number of studies have explored the properties of water for various size water pools and types of reverse micelles, including those formed with the ionic surfactants Aerosol OT (AOT),[4−6,26,27,55−60] as well as several nonionic surfactants.[61,62] The dynamics of water in nanoscopic environments have employed AOT extensively because AOT reverse micelles are very well characterized in terms of their sizes and shape in the range of water nanopools from ~1 to ~30 nm. The dynamics of water in AOT reverse micelles deviates substantially from those of the bulk water when the size of the reverse micelles becomes smaller than several nanometers. Here, small AOT reverse micelles with a water nanopool size of 1.7, 2.3, and 4 nm are discussed. In comparison to bulk water, orientational relaxation, which requires hydrogen bond network randomiza-

tion, becomes very slow and nonexponential as the size of the water nanopool is decreased.

Ionic reverse micelles such as AOT are formed from ionic surfactants with ionic head groups and counterions. As a consequence, water molecules in small ionic reverse micelles are in direct contact or close to charged interfaces. Therefore, the properties and dynamics of the nanoscopic water pools observed using ionic reverse micelles may arise from two physical factors: the effect of nanoscopic confinement and the effect of charges. Studies of ions in solution show that water dynamics are influenced by ions. To address the question of whether the change in the dynamics of water in ionic reverse micelles results from the effect of the charged interface or confinement, two different types of reverse micelles, one with ionic and one with nonionic surfactants, are compared. In contrast to AOT surfactants with ionic sulfonate head groups and sodium counterions, Igepal surfactants have a nonionic head group composed of an alcohol tethered by a polyether chain. The nonionic reverse micelle (Igepal CO 520) is the only truly well characterized system that permits a direct comparison with AOT. Orientational relaxation dynamics of water in identical 4 nm diameter nanopools in ionic ($w_0 = 10$ AOT) and nonionic ($w_0 = 7$ Igepal) reverse micelles and in 6 M NaBr solution are compared. The 6 M NaBr has a nominal ionic strength that is comparable to that of the $w_0 = 10$ AOT reverse micelle. The remarkable result is that the orientational relaxation in the two reverse micelles is almost identical and much slower than that in 6 M NaBr. The experimental observations suggest that the hydrogen bond dynamics of water in nanoconfinement arise mainly from effects of nanoscopic confinements rather than the presence of ions.

II. Experimental Procedures

A. Femtosecond Mid-Infrared System. The laser system employed in the experiments has been described in detail elsewhere.[1] Briefly, 800 nm pulses are generated by a Ti: Sapphire oscillator and regenerative amplifier laser system at 1 kHz. These pulses are used to pump an optical parametric amplifier (OPA, Spectra-Physics) to produce near-IR pulses at ~1.3 and ~2.0 μm, which are utilized to generate mid-IR pulses at ~4 μm in a 0.5 mm thick $AgGaS_2$ crystal by difference frequency generation (DFG). The power spectrum of the mid-IR pulses has a Gaussian envelope with a ~260 cm^{-1} bandwidth (full width at half-maximum). After the mid-IR pulses are generated, the experimental setup is purged with dry CO_2-scrubbed air to remove both atmospheric water and strong CO_2 absorptions. Pulse chirp is determined using FROG measurements in a transient grating geometry.[1] CaF_2 plates with different thickness are used to balance the chirp introduced by other dielectric materials in the setup, particularly a Ge Brewster plate, producing transform-limited IR pulses in the sample. Two types of third-order experiments are utilized: 2D-IR vibrational echoes and polarization-selective IR pump−probe measurements.

B. 2D-IR Vibrational Echo Experiments. Ultrafast 2D-IR vibrational echo experiments are performed by manipulating multiple pulse sequences. The details of 2D-IR experiments are described elsewhere.[1] A schematic of the experiment and the pulse sequence are shown in Figure 1. Briefly, three mid-IR pulses (wave vectors $\boldsymbol{k}_1$, $\boldsymbol{k}_2$, and $\boldsymbol{k}_3$) that can be time-delayed are focused into the sample in a noncollinear geometry. The signal is emitted in a unique phase-matched direction ($\boldsymbol{k}_s = \boldsymbol{k}_2 + \boldsymbol{k}_3 - \boldsymbol{k}_1$) and is then overlapped with a local oscillator (LO) pulse for heterodyne detection. The heterodyned signal is dispersed through a monochromator onto the top stripe of a dual 32 × 2 element mercury−cadmium−telluride (MCT) array detector (Infrared Associates and Infrared Systems Development Corp.) and is frequency-resolved. A small portion of the IR beam that does not go through the sample is sent to the bottom stripe of the array and is used as a reference beam. The mainly absorptive 2D-IR spectra are obtained by using the dual scan method in which non-rephasing and rephasing 2D-IR spectra are measured by two different input pulse sequences and added.[1,51,63]

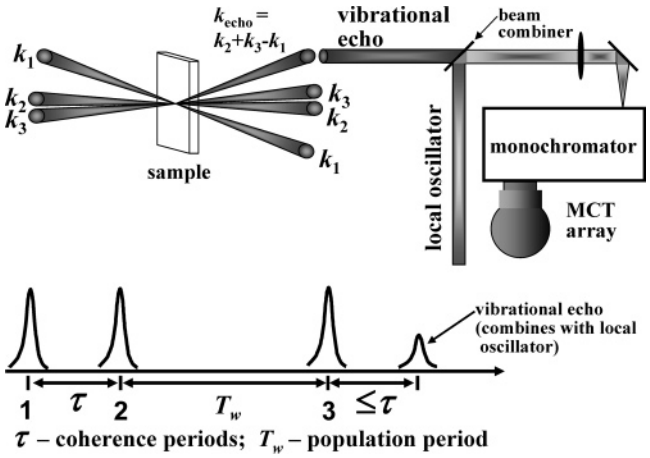

Figure 1. Schematic illustration of the 2D-IR vibrational echo experiment and pulse sequence. Three pulses enter the sample with the timing given by the pulse sequence shown at the bottom of the figure. The nonlinear interactions give rise to a fourth pulse, the vibrational echo, which is then combined with the local oscillator pulse to obtain phase and amplitude information. The combined vibrational echo and local oscillator are frequency resolved and detected with an IR MCT array. For fixed T_w, τ is scanned. The Fourier transformations produce a 2D spectrum. Spectra are recorded as a function of T_w.

In 2D-IR vibrational echo experiments, there are three time variables: evolution time, τ, waiting time, T_w, and detection time, $t \leq \tau$ (see Figure 1). The first IR pulse excites the molecules to produce coherent superposition states where the wave functions are superpositions of the $v = 0$ and 1 vibrational energy states. The first interaction (pulse) causes the molecules to "oscillate" initially in phase at their initial frequencies. The phase relationships among the molecules decay quickly because of static inhomogeneous and dynamic broadening mechanisms. The decay of the phase relationships produces a vibrational free induction decay (FID). The second IR pulse transfers the coherent state into a population state in either the $v = 0$ or $v = 1$ energy level, depending on the phase of the particular molecule at the time of the pulse. During the population period (waiting time T_w), the molecules can undergo spectral diffusion, that is, their frequencies evolve because of dynamic structural evolution of the molecular system. Spectral diffusion causes the molecules to lose memory of their initial frequencies. In the water systems discussed below, time-dependent evolution of water's hydrogen bond network causes spectral diffusion of the hydroxyl stretch vibration of water because the hydroxyl stretch frequency is sensitive to the local environments associated with the strength and number of hydrogen bonds.[9,51] The third IR pulse brings the molecules into a second coherent state where their wave functions are again superpositions of the $v = 0$ and 1 levels or between the $v = 1$ and 2 levels. During the second coherence period (detection time), the molecules oscillate at their final frequencies, which can be different from those they had during the first coherence period. The signal is emitted at a $t \leq \tau$ time later and combines with the LO for heterodyne detection; the final frequencies of the molecules are recorded.

The heterodyne detection of the signal enables recovery of the signal's amplitude, frequency, and phase. In practice, 2D-

IR vibrational echo signals are collected by scanning τ at a fixed T_w and are frequency-resolved by a monochromator. Spectral resolving of the frequencies of the combined vibrational echo/LO wavepacket performs one of the two Fourier transforms into the frequency domain. At each monochromator frequency ω_m, a time interferogram is obtained as τ is scanned as a function of τ. Time interferograms are Fourier transformed to give the ω_τ axis. 2D-IR spectra are displayed with the initial frequency axis of ω_τ (horizontal axis) and the final frequency axis of ω_m (vertical axis) at a given T_w time. Therefore, a 2D-IR vibrational echo spectrum is a 2D frequency correlation map between the initial and final frequencies of the molecules at a given T_w. 2D-IR spectra are obtained for many T_w's. The T_w dependence of the 2D-IR spectra gives the information on the dynamics of the molecular system. The 2D-IR vibrational echo experiments have been reviewed recently.[1,64,65]

Qualitatively, the pulse sequence in 2D-IR vibrational echo experiments induces and then probes the coherent evolution of excitations (vibrations) of a molecular system. The first pulse in the sequence causes vibrational modes of an ensemble of molecules to "oscillate" initially all with the identical phase. The second pulse labels the frequencies of the molecules initially excited by the first pulse. During the period between the second and third pulses, structural changes in the system cause the frequencies of the labeled molecules to change. The third pulse begins the read out of the molecular frequencies and generates the observable signal, the fourth pulse, the vibrational echo. The characteristic spectrum obtained from observing the frequencies, intensities, and phases of the vibrational echo and Fourier transformation into the frequency domain is sensitive to changes in environments of individual molecules during the experiment even though the aggregate populations in distinct environments do not change.

C. Polarization-Selective IR Pump−Probe Experiments. In IR pump−probe experiments, a pump pulse excites the molecules to the first vibrational excited state ($v = 1$), and the subsequent time evolution of the molecular system is measured by a time-delayed probe pulse. The details of the pump−probe experiments have been described elsewhere.[36] The mid-IR pulses are split into the pump and probe beams with a relative intensity of 9:1 and are focused into the sample. The probe's polarization is set to 45° relative to the pump. After the sample, the components of the probe with polarization parallel and perpendicular to the pump are selected to avoid depolarization effects due to optics in the beam path.[66] Polarizers set to parallel and perpendicular are rotated using a computer-controlled wheel. Scans alternate between parallel and perpendicular to reduce effects of long-term laser drift. After the polarizers, a half wave plate rotates the polarization of each component to 45° prior to the entrance slit of a 0.25 m monochromator so that both parallel, $S_{\parallel}(t)$, and perpendicular, $S_{\perp}(t)$, polarization scans experience the same diffraction efficiency from the monochromator grating. The spectrally resolved pump−probe signal is detected by a 32 element MCT detector (Infrared Associates and Infrared Systems Development Corp.).

D. Sample Preparation. Aerosol OT, Igepal CO 520, isooctane, cyclohexane, n-hexane, NaBr, and D_2O were obtained from Sigma-Aldrich and were used as received. A 5% HOD in H_2O stock solution was prepared by adding 2.5 wt % of D_2O to H_2O. A solution of 5% HOD in H_2O was used for 2D-IR vibrational echo and IR pump−probe measurements. The OD stretching mode of HOD in H_2O was studied to avoid vibrational excitation transfer[67,68] (Förster resonant excitation transfer[69]), which will interfere with both orientational relaxation and spectral diffusion measurements. The samples were housed in cells containing two CaF_2 windows (3 mm thick) and a Teflon spacer with a thickness adjusted to obtain optical densities in the range of 0.2−0.4 including the H_2O background absorption for all solutions studied. All experiments were conducted at 25 °C.

Aqueous NaBr Solutions: The $n = 8$, 16, and 32 NaBr solutions (approximately 6, 3, and 1.5 M NaBr solutions, respectively) were prepared by mixing 0.1, 0.05, and 0.025 mol of NaBr salt with 0.8 mol of 5% HOD in H_2O, respectively. For 2D-IR experiments, a range of 2340−2700 cm^{-1} was measured with a frequency resolution of ~6 cm^{-1}. IR pump−probe signals in aqueous NaBr solutions were detected at the absorption maximum of the OD stretch vibration for each sample.

Reverse Micelles: A 0.5 M stock solution of AOT in isooctane and a 0.3 M stock solution of Igepal CO 520 in a 50/50 wt % mixture of cyclohexane/n-hexane were prepared. The residual water content in the surfactant and oil phase was measured by Karl Fischer titration. To make reverse micelles with the desired $w_0 = [H_2O]/[\text{surfactant}]$, precise volumes of water (5% HOD in H_2O) were added to the measured quantities of each stock solution. AOT ($w_0 = 2$, 5, and 10) and Igepal ($w_0 = 7$) reverse micelles were used for IR pump−probe experiments.[3,4] The $w_0 = 10$ AOT and $w_0 = 7$ Igepal reverse micelles had the same diameter of 4 nm.[3] The size of the water nanopool was determined by the value of w_0. For AOT reverse micelles with w_0 between 2 and 20, the diameter of the water nanopool was given by $d_{AOT} = (0.9w_0 + 1.1)$ nm.[70] For Igepal reverse micelles, the diameter of the water nanopool was obtained from $d_{IG} = (0.38w_0 + 1.40)$ nm.[71] Igepal reverse micelles were not studied with small-angle neutron scattering (SANS) for sizes smaller than $w_0 = 10$. However, the SANS experimental results show that reverse micelles somewhat smaller than $w_0 = 10$ are stable, and their sizes should follow the same linear relationship.[71]

The organic solvents used for the two types of reverse micelles were chosen because these are the solvents in which the micelles have undergone the most extensive characterization. The difference in the solvents should not play a role in the water dynamics. Measurements of water dynamics in AOT reverse micelles made with the solvents isooctane and carbon tetrachloride were identical within experimental error.[4−6,55]

III. Results and Discussion

A. Aqueous NaBr Salt Solutions. Water molecules around monatomic ions provide the simplest system for the investigation of the dynamics of water in the presence of charges. Therefore, examining the dynamics of water in simple ionic solutions, such as sodium bromide (NaBr) discussed here, can provide valuable insights that will increase the understanding of chemical processes and biological systems that involve charged species in aqueous solutions. NaBr salt solutions were chosen for the initial study among aqueous halide salt solutions because the OD stretch band of HOD in the solutions shows a significant blue shift in the FT-IR spectrum compared with that of HOD in pure water, suggesting a large change in the hydrogen bond structure.

1. Linear FT-IR Spectra. The background-subtracted FT-IR spectra of the OD stretch of HOD in NaBr salt solutions and pure water are shown in Figure 2. The curves are labeled by the number of waters per NaBr, n, where $n = 8$, 16, and 32 correspond to approximately 6, 3, and 1.5 M NaBr solutions, respectively. The FT-IR absorption spectra represent a time-

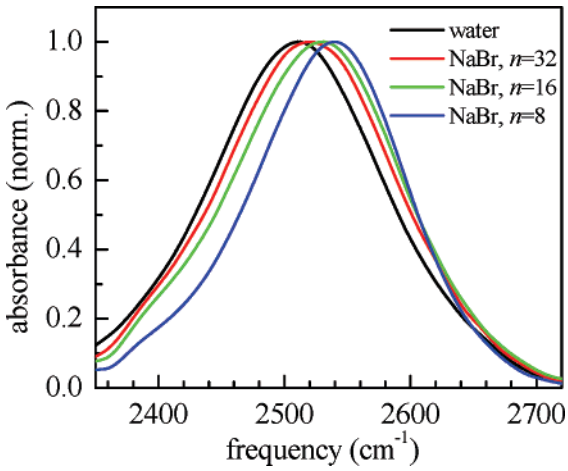

Figure 2. Absorption spectra of the OD stretch of HOD in pure water and aqueous NaBr solutions (H_2O background subtracted). The $n = 8$, 16, and 32 are the numbers of water molecules per NaBr and correspond to approximately 6, 3, and 1.5 M NaBr solutions, respectively. The peak positions (bandwidths, fwhm) of the OD stretch of HOD in pure water and $n = 32$, 16, and 8 NaBr solutions are 2509 (160), 2519 (163), 2529 (159), and 2539 cm^{-1} (141 cm^{-1}), respectively.

independent picture of the inhomogeneous distribution of the hydroxyl (OD) stretching frequencies. When a hydrogen bond is formed, the mean frequency of the hydroxyl stretch is red-shifted from the gas-phase value, its line shape broadens, and its integrated intensity increases.[72−74] The hydroxyl stretch frequency shift from its gas-phase value is mainly determined by local hydrogen bond structures, that is, the strength and number of the hydrogen bonds as well as, to some extent, the hydrogen bond angles. For pure water, it is known that the broad spectrum is associated with a wide range of strengths and different numbers of the hydrogen bonds.[10,75,76] For pure water, subensembles of water molecules with stronger and/or more hydrogen bonds have red-shifted absorptions, while subensembles with weaker and/or fewer hydrogen bonds are blue-shifted.

When ions are present, it has been shown that the hydroxyl stretch frequency is correlated with the electric field projected along the OH or OD bond vector.[77] While the electric field is the result of all of the water molecules and ions in the system, the contribution of the hydrogen bond acceptor overwhelmingly dominates. Therefore, in NaBr ionic solutions, the blue shift of the spectrum relative to that of bulk water is caused by the ODs that are hydrogen bonded to the anions. The blue shift occurs because the electric field along the OD bond is actually weaker for a hydrogen bond to Br^- than it is to an oxygen of another water molecule. The Br^- is so large and the negative charge is so diffuse that the electric field at the OD is smaller than that produced by a hydrogen bond to oxygen of another water molecule. A hydroxyl associated with I^- displays a larger blue shift, while Cl^- yields a smaller blue shift. Only F^- produces a red shift compared to bulk water because of the small size of F^-. Sodium cations have a very small or negligible effect on the hydroxyl stretch frequency because they interact with the oxygen atoms of water.[39] The spectra with K^+ cations are the same as those with Na^+.

As shown in Figure 2, FT-IR spectra of the OD stretch frequency are characteristically broad,[7,52,76] and their peak positions are increasingly blue-shifted from those of the bulk water as the NaBr concentration increases. In aqueous NaBr solutions, water molecules are hydrogen bonded to other water molecules and bromide anions. As the NaBr concentration

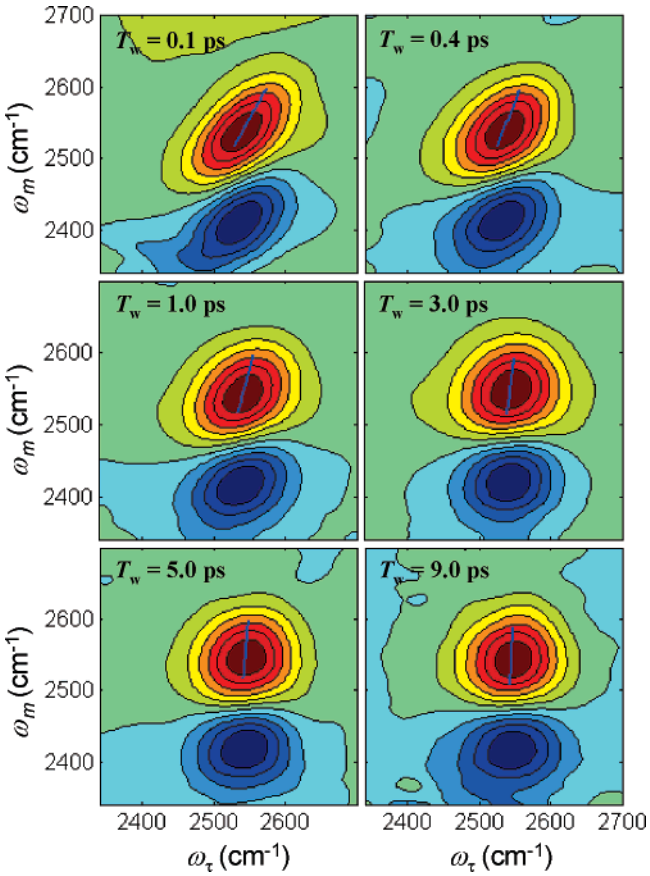

Figure 3. 2D-IR vibrational echo spectra as a function of T_w measured on the $n = 8$ (~6 M) NaBr solution. The 10% contour lines are shown. Red peaks (0−1 transition), positive going. Blue peaks (1−2 transition vibrational echo emission), negative going. The peak shape changes as T_w increases. The blue lines are the center lines.

increases, a larger fraction of the hydroxyls are associated with the Br^- ions. The spectrum is essentially a superposition of hydroxyls that are bound to other water molecules, which give a spectrum like that of pure water and hydroxyls that are bound to Br^-, which produces a blue-shifted spectrum that is substantially overlapping with the pure water spectrum. Increasing the ratio of the OD···Br^- spectrum to that of the OD···O spectrum produces a superposition spectrum that is increasingly blue-shifted.[4] FT-IR spectra of $n = 32$ and 16 NaBr solutions are well-represented by the weighted sum of spectra of bulk water and the $n = 8$ NaBr solution. This is also true for NaI solutions.

2. Hydrogen Bond Dynamics from Spectral Diffusion Measurements. 2D-IR vibrational echo spectra of the OD stretch of HOD in the $n = 8$ NaBr solution (~6 M) are shown in Figure 3 as a function of T_w. For clarity of presentation, the number of contours is limited, although the data have a far higher amplitude resolution. The red bands (on the diagonal) are positive going and result from the transition between the ground and first excited vibrational states (0−1). The blue bands (off-diagonal) are negative going and are associated with emission of the vibrational echo signal at the 1−2 transition frequency, which is shifted along the ω_m axis by the OD stretching mode anharmonicity. Focusing on the 0−1 transition (red positive band), a noticeable feature of the 2D-IR spectra is the change in shape as T_w increases. The red band is substantially elongated along the diagonal at $T_w = 0.2$ ps. As T_w increases, the shape becomes more symmetrical. This change is the signature of spectral diffusion. In the long-time limit, all structural configurations are sampled, and consequently, all frequencies are

sampled. In this limit, spectral diffusion is complete, and the peak becomes completely symmetrical. However, because of the overlap with the negative going peak that arises from emission at the 1−2 transition frequency, the bottom of the 0−1 transition band is eaten away. Spectral diffusion dynamics are obtained by analyzing the change of peak shapes as a function of T_w.

Spectral diffusion dynamics of the molecular systems can be quantified with the frequency−frequency correlation function (FFCF).[2,8,9,12,78,79] The FFCF is a key to understanding the structural evolution of molecular systems in terms of amplitudes and time scales of the dynamics. The FFCF is the joint probability distribution that the frequency has a certain initial value at $t = 0$ and another value at a later time t. The FFCF connects the experimental observables to the underlying dynamics. Once the FFCF is known, all linear and nonlinear optical experimental observables can be calculated by time-dependent diagrammatic perturbation theory.[79] Conversely, the FFCF can be determined from the 2D-IR spectra with input from the linear absorption spectrum. In hydrogen-bonded systems like aqueous solutions, the hydroxyl stretch frequency is closely related to the local hydrogen bond structure, and thus, time-dependent changes in the hydroxyl frequency (spectral diffusion) can be related to the evolution of the hydrogen bond structure.

There have been a number of methods introduced to obtain the FFCF from the results of nonlinear and linear experimental results.[80,81] Here, the center line slope (CLS) method is used to extract the FFCF from the T_w dependence of the 2D-IR spectra.[1,80] In the CLS method, frequency slices through the 2D-IR spectrum parallel to the ω_τ axis at various ω_m frequencies are projected onto the ω_τ axis.[1,2,80] These projections are a set of spectra with their peak positions at ω_τ^{max} on the ω_τ axis. The plot of ω_τ^{max} versus ω_m is a line called the center line. In Figure 3, the blue lines are the center lines for the 0−1 transition (red peaks). In the absence of a homogeneous contribution to the 2D-IR vibrational echo spectrum, the peak shape in the 2D-IR spectrum at $T_w = 0$ ps would be a line along the diagonal at 45°. The slope of this center line would be unity. At very long time, the peak shape in the 2D-IR spectrum becomes symmetrical, and the center line is vertical (slope is infinite). The inverse of the center line slope (called the CLS) varies from a maximum value of 1 at $T_w = 0$ ps to a minimum value of 0 at a sufficiently long time. It has been shown theoretically that the T_w dependence of the inverse of the center line slope combined with additional information from the absorption spectrum can be used to determine the complete FFCF.[80] Data points shown in Figure 4 are the CLS obtained from the 2D-IR spectra as a function of T_w, and the lines through data points are calculated from the FFCFs determined from the CLS and the linear FT-IR spectra.[2,80] It is clear from Figure 4 that as the concentration of NaBr increases, the spectral diffusion and, therefore, the hydrogen bond dynamics slow.

To quantify the change in dynamics with NaBr concentration, a multiexponential form of the FFCF, $C(t)$, was used to model the multitime scale dynamics of the structural evolution of the water systems.[9] The FFCF has the form

$$C(t) = \Delta_1^2 \exp(-t/\tau_1) + \Delta_2^2 \exp(-t/\tau_2) + \Delta_3^2 \exp(-t/\tau_3) \quad (1)$$

where Δ and τ are the amplitude and correlation time, respectively, of the frequency fluctuations. The τ reflects the time scale of a set of structural fluctuations, and the Δ is the range of the OD stretch frequency sampled due to the structural fluctuations. In the motionally narrowed limit (fast modulation limit) with $\Delta\tau \ll 1$, Δ and τ cannot be determined independently, but $\Delta^2\tau = 1/T_2^*$ is obtained as a single parameter describing the motionally narrowed Lorentzian contribution. T_2^* is called the pure dephasing time. The Lorentzian contribution to the 2D-IR spectrum also has contributions from lifetime (T_1) and orientational relaxation (T_{or}). The total homogeneous (Lorentzian) contribution, T_2, is given by $1/T_2 = 1/T_2^* + 1/(2T_1) + 1/(3T_{or})$, where T_2 is determined with the CLS method[1,80] and T_1 and T_{or} are measured using polarization-selective IR pump−probe experiments (see below). The total homogeneous line width is $\Gamma = 1/(\pi T_2)$. In the results presented here, Γ is dominated by the pure dephasing, T_2^*.

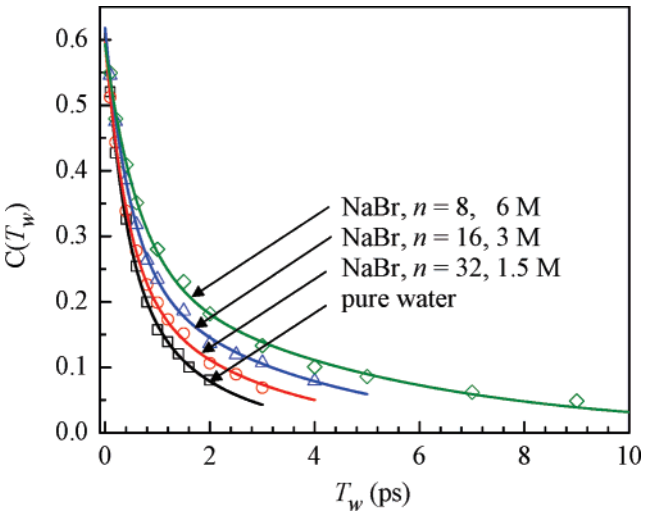

Figure 4. Spectral diffusion dynamics of the OD stretch of HOD in pure water and aqueous NaBr solutions. The data points are the inverse of the center line slope obtained from 2D-IR spectra and the line through the data points calculated from the FFCF determined from the 2D-IR spectra and linear FT-IR spectra. As the NaBr concentration increases, the dynamics of water slow.

TABLE 1: FFCF Parameters

sample	Γ (cm^{-1})	Δ_1 (cm^{-1})	τ_1 (ps)	Δ_2 (cm^{-1})	τ_2 (ps)
water	76 ± 14	41 ± 8	0.38 ± 0.08	34 ± 11	1.7 ± 0.5
$n = 32$	78 ± 9	43 ± 5	0.43 ± 0.06	34 ± 7	2.6 ± 0.5
$n = 16$	74 ± 6	41 ± 3	0.49 ± 0.05	34 ± 4	3.5 ± 0.5
$n = 8$	67 ± 6	35 ± 3	0.63 ± 0.09	30 ± 4	4.8 ± 0.6

The FFCF parameters for the aqueous NaBr solutions and pure water are given in Table 1.[2] For the motionally narrowed components, the homogeneous line width, $\Gamma = 1/(\pi T_2)$, is given. The lifetime and orientational relaxation contributions are not removed because they are very small. For example, for pure water, the combined lifetime and orientational relaxation contribution to Γ is 4 cm^{-1}, which is well within the error bars on the 76 cm^{-1} homogeneous line width. As seen in Table 1, the major change with increasing NaBr concentration is in the slowest time constant, τ_3, of the FFCF. The homogeneous line widths, Γ, of pure water, $n = 32$, and $n = 16$ NaBr solutions are identical within experimental error. Only for the $n = 8$ NaBr solution is Γ slightly smaller, and this value is within the error bars of the others. The Δ values, which give the amplitudes of the fluctuations on different time scales, are again very similar, with the $n = 8$ NaBr solution being slightly smaller. The time constants, τ_2 and τ_3, show a systematic trend; both become longer as the NaBr concentration increases. The τ_2 increases by a factor of ~1.6, while the τ_3 increases by ~3.

The simulations of pure water show that the motionally narrowed component arises from extremely fast (tens of femtoseconds) local fluctuations mainly in the hydrogen bond

length.[9] These exceedingly fast fluctuations amount to overdamped oscillations of single hydrogen bonds. There is some experimental evidence that the strongest hydrogen bonds (red side of the absorption spectrum) are slightly underdamped.[13,82] These ultrafast motions do not change the global structure of hydrogen bond networks. The slowest time (1.7 ps) for pure water is associated with the final complete randomization of the hydrogen bond structure. This is the time scale for global rearrangement of hydrogen bond networks, and it requires breaking and re-forming of hydrogen bonds as hydrogen bond partners switch. The complete structural reorganization means that the OD stretch oscillators will have sampled all structures and, therefore, all vibrational frequencies. This slowest decay time is the time scale on which spectral diffusion is complete, and all frequencies under the inhomogeneously broadened absorption spectra have been sampled. The ~400 fs time scale is a transition between the strictly local hydrogen bond length fluctuations and the final complete structural reorganization.[83] The intermediate and slowest time scale components in the FFCF should not necessarily be viewed as distinct processes.

It is useful to take the results from the MD simulations of pure water and carry them over to understanding the FFCFs obtained from highly concentrated NaBr solutions. It is reasonable to assume that the ultrafast motionally narrowed contribution to the FFCF still arises from local hydrogen bond length fluctuations. However, in highly concentrated NaBr solutions, the hydrogen bonds are no longer solely among water molecules but rather between water molecules and ions. At the highest concentration, $n = 8$, most of the OD groups will be hydrogen bond donors to bromide anions. This change in the nature of the OD hydrogen bond length fluctuations may be manifested in the reduction in Γ seen in Table 1. As mentioned above, the slowest component of the FFCF displays the largest change with increasing NaBr concentration. The slowest component slows by almost a factor of 3 going from pure water to the $n = 8$ NaBr solution. Therefore, as more and more hydrogen bonds are made to bromide anions rather than among water molecules, the rate of global structural rearrangement slows. The structural randomization is just a factor of 3 slower than that in pure water even when the number of water molecules is less than what would be required to make single hydration shells in dilute aqueous solutions.

Previously, two-color IR pump−probe experiments were performed by pumping the OH stretch of HOD in D_2O salt solutions (6 M NaCl, NaBr, or NaI) near the center of the OH stretching band and measuring vibrational population relaxation at different frequencies.[37] The results were interpreted as spectral diffusion and were analyzed in terms of a single correlation time constant τ_c. The correlation times were reported to be 20−50 times longer than those of pure water. MD simulations on halide−water systems suggested that the very long correlation times measured by two-color pump−probe experiments were similar to residence times of water molecules in the first hydration shells of halide anions in dilute solutions.[84−87] However, there is no bulk water in the highly concentrated salt solutions, and as shown in previous studies of various water systems,[4,9,13,47] the FFCFs of water are nonexponential in nature and decay on multiple time scales. A model with two subsets of water molecules, water bound to ions, and bulk water seems to be insufficient to describe the hydrogen bond dynamics of water in the very highly concentrated salt solutions.

The very long correlations times obtained from two-color pump−probe experiments are in contrast to the results obtained from the direct measurements of spectral diffusion dynamics using the 2D-IR vibrational echo experiments for the 6 M NaBr and are supported by the anisotropy decays occurring on similar time scales. Recently, MD simulations were performed on ionic solutions, and hydrogen bond lifetime correlation functions were calculated.[86,87] These simulations show that the lifetime of water−Br^- hydrogen bonds is a few picoseconds and is somewhat longer than that of water−water hydrogen bonds.[87]

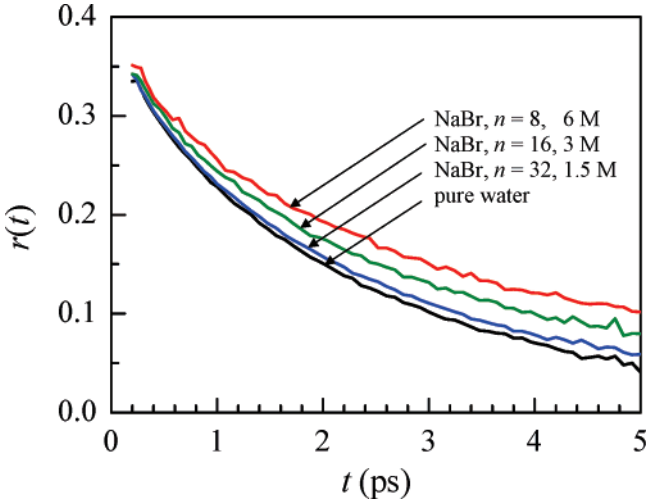

Figure 5. Anisotropy decays, $r(t)$, of the OD stretch of HOD in pure water and aqueous NaBr solutions. As the NaBr concentration increases, the orientational relaxation slows.

3. Orientational Relaxation. The parallel ($S_{||}$) and perpendicular ($S_\perp$) components of the pump−probe signal measured with two beam polarization configurations are given by

$$S_{||} = P(t)[1 + 0.8C_2(t)] \quad (2)$$

$$S_\perp = P(t)[1 - 0.4C_2(t)] \quad (3)$$

where $P(t)$ is the population relaxation and $C_2(t) = \langle P_2[\boldsymbol{\mu}(t)\cdot\boldsymbol{\mu}(0)]\rangle$ is the second-order Legendre polynomial transition dipole correlation function (orientational relaxation). Orientational relaxation dynamics are determined from the anisotropy decay, $r(t)$, that is calculated from the parallel and perpendicular components of the pump−probe signals

$$r(t) = \frac{S_{||} - S_\perp}{S_{||} + 2S_\perp} = 0.4C_2(t) \quad (4)$$

In water systems, vibrational population relaxation is followed by the deposition of heat into the solution that produces a long-lived orientationally isotropic signal.[32] This long-time isotropic signal, which decays on thermal diffusion time scales, is caused by the temperature dependence of the water spectrum. The magnitude of the temperature change in these experiments is small (fraction of 1 K). The heating effects are well-understood and are subtracted from the pump−probe signals using the standard procedure.[4,32,88] The vibrational population relaxation of the OD stretch of HOD in aqueous NaBr solutions is well-fit by a biexponential function and gets slower with increasing NaBr concentrations.[2]

Figure 5 displays the anisotropy decays, $r(t)$, for pure water and aqueous NaBr solutions. As the NaBr concentration increases, the orientational relaxation slows. The anisotropy decays do not begin at the maximum value of 0.4 (see eq 4) because of an ultrafast inertial component that occurs on the tens of femtoseconds time scales.[5,33,89] For times < 100 fs, when the pump and probe pulses are overlapped in time, there is a

large nonresonant signal that obscures the inertial component. The difference in the amplitude of the measured anisotropy decay and 0.4 gives a measure of the amplitude of the inertial component. In the following, only the anisotropy decay after the inertial component is discussed.

The anisotropy decay of HOD in pure water is a single exponential with a time constant of 2.6 ps.[4,33] However, the anisotropy decays of water in aqueous NaBr solutions are clearly not single exponential and are fit very well by a biexponential function of the form

$$r(t) = a_1 \exp(-t/\tau_{or1}) + a_2 \exp(-t/\tau_{or2}) \qquad (5)$$

where $\tau_{or2} > \tau_{or1}$. Water molecules in NaBr solutions are hydrogen bonded to bromide anions by strong ion−dipole interactions. These ion−dipole interactions restrict orientational motions of water in NaBr solutions. Experiments on HOD in water nanopools in small AOT reverse micelles[4−6] (discussed below) and in nanoscopic water channels in Nafion fuel cell membranes[36] also displayed biexponential decays of the anisotropy. The biexponential decays of the anisotropy in NaBr solutions are analyzed by a wobbling-in-a-cone model based on restricted orientational diffusion with a boundary condition of a cone[90] followed by complete randomization.[4,5,36] The motions at short times are restricted by the intact hydrogen bond network. Orientational diffusion occurs by the wobbling motion of water within a cone of the semiangle of θ_c. After the initial wobbling period, a longer-time decay of the anisotropy is associated with complete orientational randomization. The essential idea is that on a time scale short compared to that for the rearrangement of the hydrogen bond structure (breaking and re-forming of hydrogen bonds), the OD bond vector, which is essentially the transition dipole vector, can sample a restricted range of orientations but cannot completely randomize. In pure water, the wobbling motion and overall orientational relaxation seem to occur on similar time scales and cannot be separated in time as distinct processes. As a result, within experimental error, the anisotropy decay in pure water is a single exponential after the ultrafast inertial component.

Recent molecular dynamics simulations have shown that the orientational relaxation of water molecules in pure water and ionic solutions is described by a jump reorientation model rather than Gaussian orientational diffusion.[54,91] Water molecules undergo complete randomization of their orientations by switching their hydrogen bond partners in a concerted manner, which involves large angular jumps. This model was recently applied to nanoscopic water in Nafion fuel cell membranes.[36]

In the wobbling-in-a-cone model, the orientational correlation function is given by

$$C_2(t) = [S^2 + (1 - S^2) \exp(-t/\tau_w)] \exp(-t/\tau_l) \qquad (6)$$

where S ($0 \le S \le 1$) is the generalized order parameter that describes the degree of restriction of the orientational motion, τ_w is the time constant of the wobbling-in-a-cone motion, and τ_l is the time constant for the long-time complete orientational relaxation.[4,36,90] By comparing eqs 5 and 6, $\tau_w = (\tau_{or1}^{-1} - \tau_{or2}^{-1})^{-1}$, $\tau_l = \tau_{or2}$, and $S = \sqrt{a_2}$. The cone semiangle θ_c is obtained from the generalized order parameter, $S = 0.5 \cos\theta_c(1 + \cos\theta_c)$.

The parameters from fitting the anisotropy decays with eqs 5 and 6 are given in Table 2. In the absence of the ultrafast inertial component, $a_1 + a_2 = 0.4$. The decrease from 0.4 gives the amplitude of the ultrafast inertial component. For the three NaBr solutions, the wobbling time constant τ_w and cone semiangle θ_c are identical. However, the long time constant, τ_l, increases as the NaBr concentration increases. In the $n = 8$ NaBr solution, τ_l is almost three times longer than that in pure water. Like the slowest component of the spectral diffusion (see Table 1), the complete randomization of the OD transition dipoles requires a global reorganization of the hydrogen bond structure.

TABLE 2: Orientational Relaxation Parameters

sample	a_1	τ_w (ps)	θ_c (°)	a_2	τ_l (ps)
water				0.35 ± 0.01	2.6 ± 0.1
$n = 32$ NaBr	0.16 ± 0.02	1.7 ± 0.2	38 ± 4	0.21 ± 0.03	3.9 ± 0.3
$n = 16$ NaBr	0.17 ± 0.03	1.6 ± 0.1	38 ± 2	0.21 ± 0.01	5.1 ± 0.2
$n = 8$ NaBr	0.17 ± 0.01	1.6 ± 0.1	38 ± 2	0.21 ± 0.01	6.7 ± 0.3
AOT $w_0 = 10$	0.12 ± 0.01	1.5 ± 0.2	31	0.25 ± 0.01	22 ± 1
AOT $w_0 = 5$	0.08	1.0	31	0.25	30
AOT $w_0 = 2$	0.03	0.9	29	0.27	50
Igepal $w_0 = 7$	0.10 ± 0.01	1.6 ± 0.2	32	0.24 ± 0.01	21 ± 1

While the FFCF and the orientational correlation function cannot be directly compared, the physical picture states that the slowest component of each requires complete rearrangements of the hydrogen bond structure. It is useful to compare the effect of NaBr concentration on the slowest components of the FFCF and orientational correlation function shown in Tables 1 and 2, respectively. This can be done by taking the ratios, R, of the time constants of the slowest components for NaBr solutions with respect to the value for pure water. For the FFCF, $R_{FFCF} = 1.5$, 2.1, and 2.8 going from low to high concentration. For the orientational correlation function, $R_{or} = 1.5$, 2.0, and 2.6. These ratios are identical within experimental error. The identical trend in the two ratios strongly supports the picture that the slowest components of both experimental observables are closely related to the global rearrangement of the hydrogen bond structure, which occurs by concerted breaking and re-forming of the hydrogen bonds. The results of the 2D-IR vibrational echo and pump−probe experiments demonstrate that the interaction of water with ions slows the structural rearrangement of water, but even in the 6 M NaBr solution, the reduction is only a factor of ~3.

B. Reverse Micelles. Reverse micelles are useful systems for studying the effects of nanoscopic confinement on water dynamics. A reverse micelle is composed of amphiphilic surfactant molecules self-assembled such that they form a closed structure with polar or charged head groups pointing inward, toward the polar water phase, while hydrocarbon chains are pointing outward toward the nonpolar phase. AOT reverse micelles have been studied extensively by many experimental methods to understand the properties and dynamics of confined water on nanometer length scales.[4−6,26,27,55−59,92] Ultrafast IR experiments investigate the dynamics of nanoscopically confined water by making measurements directly on the water molecules rather than examining the properties of a fluorescent dye molecule or other types of probe molecules located in the water nanopool. This section focuses on the influence of confinement on FT-IR spectra and orientational relaxation dynamics of water in small AOT reverse micelles.[4−6,55] Vibrational echo experiments have also been conducted on water in AOT reverse micelles.[4,6] As shown above, polarization-selective pump−probe measurements of orientational relaxation and vibrational echo measurements of spectral diffusion provide complementary information. In the interest of brevity, only the orientational relaxation measurements will be discussed here.

1. Linear FT-IR Spectra. AOT reverse micelles were studied with $w_0 = 60$, 40, 20, 10, 5, and 2.[4] These range in diameter of the water nanopools from 28 down to 1.7 nm. Here, the smallest of the reverse micelles are discussed because they display the

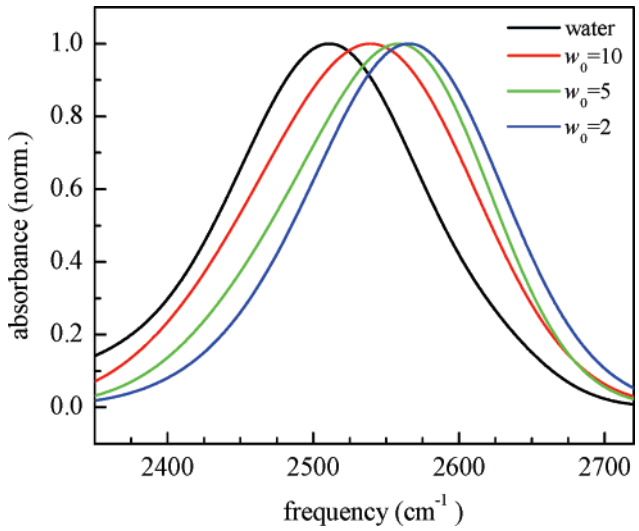

Figure 6. Absorption spectra of the OD stretch of HOD in water nanopools of AOT reverse micelles and in bulk water. The $w_0 = 2$, 5, and 10 correspond to the reverse micelle sizes 1.7, 2.3, and 4 nm, respectively. The peak positions (bandwidths (in fwhm)) of the OD stretch of HOD in $w_0 = 2$, 5, and 10 AOT reverse micelles are 2565 (155), 2559 (161), and 2537 cm^{-1} (177 cm^{-1}), respectively.

most dramatic differences from bulk water. Figure 6 shows the background-subtracted FT-IR spectra of the OD stretch of HOD in water of bulk water and in AOT reverse micelles with $w_0 =$ 10, 5, and 2, which correspond to nanopool diameters of 4, 2.3, and 1.7 nm and the number of water molecules, ~1000, ~300, and ~40, respectively. The peak positions (bandwidths, fwhm) for $w_0 = 10$, 5, and 2 are 2537 (177), 2559 (161), and 2565 cm^{-1} (155 cm^{-1}), respectively, with water centered at 2509 cm^{-1}. It is clear that the FT-IR spectrum increases its blue shift from that of bulk water as the size of the water nanopool decreases. AOT surfactants have an ionic sulfonate head group with a sodium counterion. In $w_0 = 2$ with only ~40 water molecules, essentially all of the water molecules are associated with the sulfonate head groups of the AOT surfactants. The FT-IR spectrum for $w_0 = 2$ is blue-shifted from the bulk spectrum by ~55 cm^{-1}. This large change in the OD stretch frequency is related to the electric field projected onto the OD bond vector.[77] As the AOT reverse micelles get smaller, the relative number of water molecules associated with the sulfonate head groups increases, and the FT-IR spectra becomes increasingly blue-shifted. This is the same type of shift observed in Figure 2 as the concentration of NaBr is increased.

In AOT reverse micelles, water molecules can be divided into two subensembles in a core−shell model.[4] Water molecules associated with the sulfonate head groups form the shell, and the water molecules some distance in from the sulfonate head groups form the core. Water molecules in core have the same OD absorption spectrum as that for bulk water.[4] FT-IR spectra of the OD stretch in the water nanopools of $w_0 = 5$ and 10 AOT reverse micelles can be reproduced with great accuracy (peak position, line width, and shape) using a weighted sum of the FT-IR spectra of bulk water and $w_0 = 2$. For any size AOT reverse micelles, the FT-IR spectrum is composed of a core spectrum (bulk water spectrum) and a shell spectrum (spectrum of $w_0 = 2$).[4]

It should be mentioned that vibrational population relaxation of the OD hydroxyl stretch of water in the AOT reverse micelles was observed to be biexponential, with the overall decay becoming longer as the size of the reverse micelles decreases.[4] For any size reverse micelle, the biexponential decay of

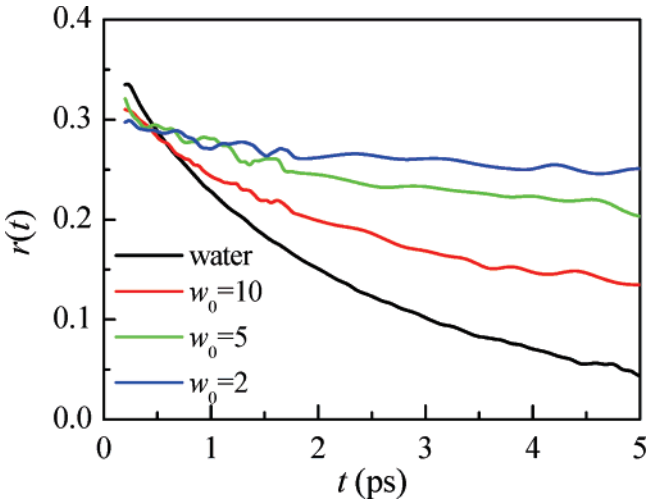

Figure 7. Anisotropy decays, $r(t)$, of the OD stretch of HOD in water nanopools in AOT reverse micelles with different water nanopool sizes. As the size of the reverse micelles decreases, the orientational relaxation slows.

vibrational population can be described by the weighted sum of a core lifetime (bulk water, 1.7 ps) and the shell lifetime. The shell lifetime is taken to be the single-exponential lifetime, 5.2 ps, measured for $w_0 = 2$, which is so small that essentially all of the water molecules are associated with head groups (the shell).[4]

2. Orientational Relaxation. The anisotropy decays of water in AOT reverse micelles with different nanopool sizes and bulk water are shown in Figure 7. The probe signal was detected at the wavelength of the peak of each spectrum. The anisotropy decay slows dramatically as the size of the reverse micelles decreases. As discussed above in connection with the NaBr experiments, complete orientational relaxation requires hydrogen bond randomization. Therefore, as the size of the water nanopool decreases, hydrogen bond dynamics slow. It has been found that the hydrogen bond dynamics of water approach those of bulk water as the size of AOT reverse micelles is increased significantly above 4 nm ($w_0 = 10$).[4]

Orientational relaxation of water in reverse micelles is well-characterized by a biexponential function and is analyzed using the wobbling-in-a-cone model (eqs 5 and 6). The results are given in Table 2. The most notable change in the anisotropy decay with decreasing nanopool size is in the long-time dynamics that are associated with the global rearrangement of the hydrogen bond structure. Orientational dynamics of water in reverse micelles cannot be described by a weighted sum of two subensembles of water molecules (core and shell), in contrast to the FT-IR spectra and vibrational population decays.[4] The core and shell regions, while physically distinct, are intimately connected through the hydrogen bond network. Simulations[89,93,94] and physical considerations[5,6] show that the Na^+ counterions are associated with the sulfonate anionic head groups. While the detailed structure of water associated with the head group/counterion is unknown, it is safe to say that the arrangement of water molecules in a shell of waters at the interface will differ substantially from that of bulk water.

Consider a hypothetical system possessing an infinite extent of water molecules with the structure found near the interface. Such a system will have global hydrogen bond network randomization dynamics that are different from those of the bulk water. If this infinite extent shell structure could be in contact with an infinite bulk water system, at the boundary between the two, there would have to be accommodation akin to the

interface of two incommensurate crystal lattices. When two incommensurate crystal lattices are joined, the structure of the boundary region differs from that of both pure crystalline materials because of accommodation.[95] However, if the two types of crystals are macroscopic in extent, at some distance from the boundary, their unperturbed lattice structures will exist. In the reverse micelle, a thin shell layer meets a relatively small core region. In isolation, the structures of these regions differ, but their structures and particularly their long-time-scale global hydrogen bond dynamics are strongly coupled. Because core waters are hydrogen bonded to shell waters, the rearrangements responsible for full orientational relaxation in the small reverse micelles require motions that depended on the structure of the coupled system. The influence of the interface will extend some distance into the core. If the water nanopool is small enough, the hydrogen bond dynamics will not become those of bulk water anywhere. The influence of the interface on dynamics is different from that of the spectrum and the population relaxation. Both the spectrum and the population relaxation are completely dominated by the local structure, in contrast to the hydrogen bond rearrangement, which requires global structural changes that are not strictly local. The hydrogen bond dynamics are not necessarily uniform throughout the water nanopool in small AOT reverse micelles, as has been shown by a wavelength dependence of the orientational relaxation.[34]

C. The Role of Confinement versus Charge on the Dynamics of Water. The dynamics of water in anionic AOT reverse micelles are distinct from those of the bulk water. Water dynamics also differ from those of the bulk water in concentrated NaBr solutions in which the number of water molecules per ion is similar to that in the reverse micelles studied. Therefore, the fundamental question arises, are the large changes in hydrogen bond dynamics found in the experiments with AOT reverse micelles caused by nanoscopic confinement or by the presence of the charged sulfonate head groups?[3]

The issue of confinement versus charge can be addressed by comparing the experimental results obtained for AOT water nanopools to those for a reverse micelle made from a nonionic surfactant. In spite of a wide variety of nonionic surfactant/organic phase combinations, no one combination has been as thoroughly studied and characterized as the AOT reverse micelle system. Of the many combinations, a well-characterized nonionic reverse micelle can be made of the surfactant Igepal CO 520 with an organic phase consisting of a 50/50 by weight mixture of cyclohexane and n-hexane.[96] This alcohol head group nonionic surfactant and organic phase combination was chosen because the resulting reverse micelles have been studied in detail by small-angle neutron scattering (SANS) to determine their structure.[96] The stability regime of the reverse micelle phase was mapped out, and the water pool sizes were determined at a number of temperatures and w_0 values. In addition, the SANS fitting indicated a spherical shape for the reverse micelles, and molecular dynamics simulations on a similar system showed only a slight ellipticity.[97] The combination of spherical shape and relatively good size characterization makes this Igepal system useful for comparison with the AOT reverse micelle system. Because of a lack of a similar detailed characterization of other nonionic reverse micelles, the Igepal system is the only system suitable for these studies.[3]

Igepal reverse micelles with $w_0 = 7$ were studied.[3] For $w_0 = 7$, an Igepal reverse micelle nanoscopic water nanopool is the same size as the AOT $w_0 = 10$ reverse micelle, that is, $d = 4$ nm.[3,96] A diameter of 4 nm was chosen because in previous studies of nanoscopic water in AOT, the $w_0 = 10$ reverse micelle was shown to have water dynamics significantly different from those of bulk water, as can be seen in Figure 7. AOT reverse micelles have water dynamics that rapidly approach those of bulk water as the size is increased beyond 4 nm.[4] Therefore, significantly larger sizes are not useful.

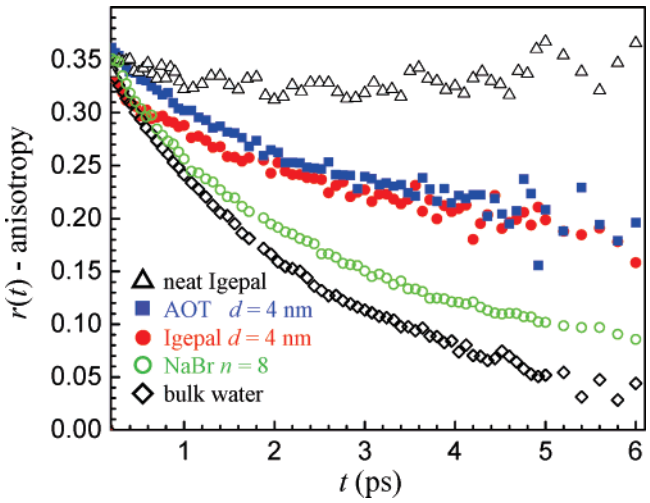

Figure 8. Anisotropy decays, $r(t)$, of the OD stretch of HOD in water nanopools of Igepal and AOT reverse micelles with the same water nanopool size of 4 nm. Anisotropy decays of the OD stretch of HOD in pure water and in the $n = 8$ NaBr solution (6 M), as well as for the hydroxyl head groups (5% OD) of pure Igepal, are also shown for comparison.

Smaller sizes are problematic for two important reasons. First, the size of smaller Igepal reverse micelles becomes increasingly uncertain as the size is decreased. Second, the deuterium from a HOD molecule will exchange with the Igepal hydroxyl group so that instead of studying only water, the experiment also has a contribution from the hydroxyl group of Igepal. This is a real effect, but it will only be significant for very small reverse micelles in which the number of surfactant molecules is comparable to the number of water molecules. For the $w_0 = 7$ reverse micelle, there are 7 water molecules per surfactant molecule, which means that there are 14 water hydroxyl groups for each Igepal hydroxyl group. Statistically, the contribution to the signal from a water OD stretch will outweigh the Igepal hydroxyl OD by a factor of 14.

Therefore, comparing 4 nm AOT and Igepal reverse micelle water nanopools to understand the effects of interfacial differences on the dynamics of the confined water is appropriate, and this is essentially the only size that can provide well-defined results to answer the question of whether or not interfacial charges dictate the dynamics of confined water. A single counter example is sufficient to demonstrate that interfacial charges are not solely responsible for confinement effects on water dynamics.

FT-IR spectra of the OD stretch of HOD in water in Igepal $w_0 = 7$ is shifted to the blue of bulk water but not as much in AOT $w_0 = 10$. The Igepal maximum is at 2522 cm^{-1}, while the AOT maximum is at 2537 cm^{-1}, which is almost identical to the peak of the spectrum of the $n = 8$ NaBr solution. The OD in bulk water maximum is at 2509 cm^{-1}. In the Igepal reverse micelles, water molecules at the surfactant interface are hydrogen bonded to the alcohol hydroxyl head group, while in AOT and the concentrated NaBr solution, water is hydrogen bonded to ions. This difference is responsible for the reduction in the blue shift for Igepal compared to that for AOT and the NaBr solution.

Figure 8 displays the anisotropy decays of the OD stretch of HOD in water nanopools with a diameter of 4 nm in AOT and Igepal reverse micelles measured at the same wavelength, 2539 cm^{-1}, close to the peak of both spectra. The anisotropy decays

of bulk water, the $n = 8$ NaBr solution, and pure Igepal surfactant are also shown in Figure 8 for comparison. The orientational relaxation dynamics in these two reverse micelles are very similar and much slower than those in bulk water. The anisotropy decays in both reverse micelles are biexponential, and the two components are identical within experimental error (see Table 2). The difference in the appearance of the AOT and Igepal curves comes from the very short time inertial component. AOT displays a much smaller ultrafast (<100 fs) inertial decay component than that of Igepal. In contrast to the reverse micelles, bulk water's anisotropy decay is a single exponential of 2.6 ps. The anisotropy decay of the $n = 8$ NaBr solution, while slower than that of bulk water, is much faster than the orientational relaxation of water in the reverse micelles. The anisotropy of neat Igepal surfactants is essentially constant for the time window of pump−probe experiments, which shows that the orientational dynamics measured for the Igepal reverse micelle are not dominated by the Igepal hydroxyl groups.[3]

The key finding is that the orientational dynamics of water are very similar in 4 nm diameter Igepal ($w_0 = 7$) and AOT ($w_0 = 10$) reverse micelles even though the two types of reverse micelles have different head groups (nonionic vs ionic) that interact with water molecules at the interfaces in the shell region. As shown in Figure 8, the orientational dynamics of water in the $w_0 = 10$ AOT reverse micelle are much slower than those in the $n = 8$ NaBr solution. It should be noted that the spectral diffusion of water in the $w_0 = 10$ AOT reverse micelle measured by vibrational echo experiments is substantially slower than that in the $n = 8$ NaBr solution.[2,4] The ionic strengths in these samples are approximately the same, but they have different ionic structures. In the $n = 8$ NaBr solution, there are four water molecules per ion, and as a result, the water molecules in the NaBr solution are all in close proximity to bromide anions and sodium cations. In the $w_0 = 10$ AOT reverse micelle, over 50% of the water molecules in the core and are not associated with anionic sulfonate/sodium cation head groups of the AOT surfactants in the shell region.[4]

It can be inferred from these facts and the anisotropy decays shown in Figure 8 that the substantial slowing of the hydrogen bond dynamics in AOT reverse micelles is not predominately a result of charges at the interface. The results from $w_0 = 10$ AOT and $w_0 = 7$ Igepal micelles as well as the ~6 M NaBr solution provide strong evidence that the modification of the dynamics of water in small reverse micelles comes mainly from the effects of the nanoconfinement; the charged interface has less influence.

IV. Concluding Remarks

A persistent question surrounding the study of water in confined environments or near interfaces has been, "is it the *presence* of or the *nature* of the confining interface that has the largest effect on the dynamics of the water molecules?" The material presented above examines the influences of ions in aqueous solutions and nanoconfinement in reverse micelles with ionic and nonionic surfactants on water dynamics. The results show that the presence of ions has a significant influence on water hydrogen bond dynamics, but the effects of an interface and confinement go well beyond the proximity of water molecules to charges that may be located at the interface.

Many important phenomena take place in nanoscopic water environments and with water at or near an interface. Biological processes occur in very crowded aqueous surroundings, with the solvating water often playing an important role. Water inside of cells and between cells experiences numerous interfaces that can be separated by a few nanometers to a few tens of nanometers. Cell membranes have zwitterions at their interfaces with water, and transmembrane protein ion channels experience water at their entrances that is distinct from bulk water. The surfaces of proteins have charged and polar amino acids forming the interface with water. Some proteins enclose water in nanoscopic compartments. Water confined on nanometer length scales is also found in many nonbiological situations. Polyelectrolyte fuel cell membranes, such as Nafion, have water-containing nanoscopic channels that have a major impact on water dynamics[3,4] and proton transport.[98,99]

The frequent incidence of nanoscopically confined and restricted water brings to the forefront the need to understand the properties of water and aqueous systems in environments near interfaces. The results presented above show that while charged species at an interface may matter, the very existence of an interface can have a profound influence on water dynamics even in the absence of ionic groups.

Acknowledgment. This work was supported by grants from the Department of Energy (DE-FG03-84ER13251), the Air Force Office of Scientific Research (F49620-01-1-0018), the National Science Foundation (DMR 0652232), and the National Institutes of Health (2 R01 GM-061137-05).

References and Notes

(1) Park, S.; Kwak, K.; Fayer, M. D. *Laser Phys. Lett.* **2007**, *4*, 704.
(2) Park, S.; Fayer, M. D. *Proc. Nat. Acad. Sci., U.S.A.* **2007**, *104*, 16731.
(3) Moilanen, D. E.; Levinger, N.; Spry, D. B.; Fayer, M. D. *J. Am. Chem. Soc.* **2007**, *129*, 14311.
(4) Piletic, I.; Moilanen, D. E.; Spry, D. B.; Levinger, N. E.; Fayer, M. D. *J. Phys. Chem. A* **2006**, *110*, 4985.
(5) Tan, H.-S.; Piletic, I. R.; Fayer, M. D. *J. Chem. Phys.* **2005**, *122*, 174501(9).
(6) Tan, H.-S.; Piletic, I. R.; Riter, R. E.; Levinger, N. E.; Fayer, M. D. *Phys. Rev. Lett.* **2005**, *94*, 057405.
(7) Lawrence, C. P.; Skinner, J. L. *J. Chem. Phys.* **2003**, *118*, 264.
(8) Asbury, J. B.; Steinel, T.; Stromberg, C.; Corcelli, S. A.; Lawrence, C. P.; Skinner, J. L.; Fayer, M. D. *J. Phys. Chem. A* **2004**, *108*, 1107.
(9) Asbury, J. B.; Steinel, T.; Kwak, K.; Corcelli, S. A.; Lawrence, C. P.; Skinner, J. L.; Fayer, M. D. *J. Chem. Phys.* **2004**, *121*, 12431.
(10) Eaves, J. D.; Loparo, J. J.; Fecko, C. J.; Roberts, S. T.; Tokmakoff, A.; Geissler, P. L. *Proc. Natl. Acad. Sci., U.S.A.* **2005**, *102*, 13019.
(11) Eaves, J. D.; Tokmakoff, A.; Geissler, P. L. *J. Phys. Chem. A.* **2005**, *109*, 9424.
(12) Fecko, C. J.; Loparo, J. J.; Roberts, S. T.; Tokmakoff, A. *J. Chem. Phys.* **2005**, *122*, 054506.
(13) Fecko, C. J.; Eaves, J. D.; Loparo, J. J.; Tokmakoff, A.; Geissler, P. L. *Science* **2003**, *301*, 1698.
(14) Schuster, P.; Zundel, G.; Sandorfy, C. *The Hydrogen Bond. Recent Developments in Theory and Experiments*; North Holland: Amsterdam, The Netherlands, 1976.
(15) Endom, L.; Hertz, H. G.; Thul, B.; Zeidler, M. D. *Ber. Bunsen-Ges.* **1967**, *71*, 1008.
(16) Ramsay, J. D. F.; Poinsignon, C. *Langmuir* **1987**, *3*, 320.
(17) Bellissentfunel, M. C.; Chen, S. H.; Zanotti, J. M. *Phys. Rev. E* **1995**, *51*, 4558.
(18) Kropman, M. F.; Bakker, H. J. *J. Chem. Phys.* **2001**, *115*, 8942.
(19) Mitra, S.; Mukhopadhyay, R.; Tsukushi, I.; Ikeda, S. J. *Phys.: Condens. Matter* **2001**, *13*, 8455.
(20) Zhu, Y.; Granick, S. *Phys. Rev. Lett.* **2001**, *87*, 096104.
(21) Levinger, N. E. *Science* **2002**, *298*, 1722.
(22) Liu, L.; Faraone, A.; Mou, C.-Y.; Yen, C.-W.; Chen, S.-H. *J. Phys.: Condens. Matter* **2004**, *16*, S5403.
(23) Floquet, N.; Coulomb, J. P.; Dufau, N.; Andre, G.; Kahn, R. *Physica B* **2004**, *350*, 265.
(24) Raviv, U.; Perkin, S.; Laurat, P.; Klein, J. *Langmuir* **2004**, *20*, 5322.
(25) Halle, B. *Philos. Trans. R. Soc. London, Ser. B* **2004**, *359*, 1207.
(26) Cringus, D.; Lindner, J.; Milder, M. T. W.; Pshenichnikov, M. S.; Vohringer, P.; Wiersma, D. A. *Chem. Phys. Lett.* **2005**, *408*, 162.
(27) Dokter, A. M. Woutersen, S.; Bakker, H. J. *Proc. Nat. Acad. Sci., U.S.A.* **2006**, *103*, 15355.
(28) Lisitza, N.; Bryant, R. G. *J. Chem. Phys.* **2007**, *126*, 101102.

(29) Woutersen, S.; Emmerichs, U.; Nienhuys, H.-K.; Bakker, H. J. *Phys. Rev. Lett.* **1998**, *81*, 1106.
(30) Laenen, R.; Simeonidis, K.; Laubereau, A. *J. Phys. Chem. B* **2002**, *106*, 408.
(31) Woutersen, S.; Emmerichs, U.; Bakker, H. J. *Science* **1997**, *278*, 658.
(32) Steinel, T.; Asbury, J. B.; Zheng, J. R.; Fayer, M. D. *J. Phys. Chem. A* **2004**, *108*, 10957.
(33) Rezus, Y. L. A.; Bakker, H. J. *J. Chem. Phys.* **2005**, *123*, 114502.
(34) Rezus, Y. L. A.; Bakker, H. J. *J. Chem. Phys* **2006**, *125*, 144512.
(35) Piletic, I. R.; Moilanen, D. E.; Levinger, N. E.; Fayer, M. D. *J. Am. Chem. Soc.* **2006**, *128*, 10366.
(36) Moilanen, D. E.; Piletic, I. R.; Fayer, M. D. *J. Phys. Chem. C* **2007**, *111*, 8884.
(37) Kropman, M. F.; Bakker, H. J. *Science* **2001**, *291*, 2118.
(38) Kropman, M. F.; Nienhuys, H. K.; Bakker, H. J. *Phys. Rev. Lett.* **2002**, *88*, 0776011.
(39) Omta, A. W.; Kropman, M. F.; Woutersen, S.; Bakker, H. J. *Science* **2003**, *301*, 347.
(40) Kropman, M. F.; Bakker, H. J. *J. Am. Chem. Soc.* **2004**, *126*, 9135.
(41) Zimdars, D.; Tokmakoff, A.; Chen, S.; Greenfield, S. R.; Fayer, M. D.; Smith, T. I.; Schwettman, H. A. *Phys. Rev. Lett.* **1993**, *70*, 2718.
(42) Tokmakoff, A.; Fayer, M. D. *Acc. Chem. Res.* **1995**, *28*, 437.
(43) Rector, K. D.; Kwok, A. S.; Ferrante, C.; Tokmakoff, A.; Rella, C. W.; Fayer, M. D. *J. Chem. Phys.* **1997**, *106*, 10027.
(44) Hamm, P.; Lim, M.; Hochstrasser, R. M. *Phys. Rev. Lett.* **1998**, *81*, 5326.
(45) Merchant, K. A.; Thompson, D. E.; Fayer, M. D. *Phys. Rev. Lett.* **2001**, *86*, 3899.
(46) Asbury, J. B.; Steinel, T.; Stromberg, C.; Gaffney, K. J.; Piletic, I. R.; Goun, A.; Fayer, M. D. *Chem. Phys. Lett.* **2003**, *374*, 362.
(47) Stenger, J.; Madsen, D.; Hamm, P.; Nibbering, E. T. J.; Elsaesser, T. *J. Phys. Chem. A.* **2002**, *106*, 2341.
(48) Zanni, M. T.; Hochstrasser, R. M. *Curr. Opin. Struct. Biol.* **2001**, *11*, 516.
(49) Zanni, M. T.; Asplund, M. C.; Hochstrasser, R. M. *J. Chem. Phys.* **2001**, *114*, 4579.
(50) Loparo, J. J.; Roberts, S. T.; Tokmakoff, A. *J. Chem. Phys* **2006**, *125*, 194521.
(51) Asbury, J. B.; Steinel, T.; Fayer, M. D. *J. Lumin.* **2004**, *107*, 271.
(52) Moller, K.; Rey, R.; Hynes, J. *J. Phys. Chem. A* **2004**, *108*, 1275.
(53) Schmidt, J. R.; Corcelli, S. A.; Skinner, J. L. *J. Chem. Phys.* **2005**, *123*, 044513(13).
(54) Laage, D.; Hynes, J. T. *Science* **2006**, *311*, 832.
(55) Piletic, I. R.; Tan, H.-S.; Fayer, M. D. *J. Phys. Chem. B* **2005**, *109*, 21273.
(56) Riter, R. E.; Undiks, E. P.; Levinger, N. E. *J. Am. Chem. Soc.* **1998**, *120*, 6062.
(57) Riter, R. E.; Willard, D. M.; Levinger, N. E. *J. Phys. Chem. B* **1998**, *102*, 2705.
(58) Deak, J. C.; Pang, Y.; Sechler, T. D.; Wang, Z.; Dlott, D. D. *Science* **2004**, *306*, 473.
(59) Patzlaff, T.; Janich, M.; Seifert, G.; Graener, H. *Chem. Phys.* **2000**, *261*, 381.
(60) Nocek, J. M.; Hatch, S. L.; Seifert, J. L.; Hunter, G. W.; Thomas, D. D.; Hoffman, B. M. *J. Am. Chem. Soc* **2002**, *124*, 9404.
(61) Zhong, Q.; Baronavski, A. P.; Owrutsky, J. C. *J. Chem. Phys.* **2003**, *119*, 9171.
(62) Sando, G. M.; Dahl, K.; Owrutsky, J. C. *J. Phys. Chem. A.* **2004**, *108*, 11209.
(63) Khalil, M.; Demirdoven, N.; Tokmakoff, A. *Phys. Rev. Lett.* **2003**, *90*, 047401(4).
(64) Finkelstein, I. J.; Zheng, J.; Ishikawa, H.; Kim, S.; Kwak, K.; Fayer, M. D. *Phys. Chem. Chem. Phys.* **2007**, *9*, 1533.
(65) Zheng, J.; Kwak, K.; Fayer, M. D. *Acc. Chem. Res.* **2007**, *40*, 75.
(66) Tan, H.-S.; Piletic, I. R.; Fayer, M. D. *J. Opt. Soc. Am. B* **2005**, *22*, 2009.
(67) Woutersen, S.; Bakker, H. J. *Nature* **1999**, *402*, 507.
(68) Gaffney, K. J.; Piletic, I. R.; Fayer, M. D. *J. Chem. Phys.* **2003**, *118*, 2270.
(69) Gochanour, C. R.; Fayer, M. D. *J. Phys. Chem.* **1981**, *85*, 1989.
(70) Kinugasa, T.; Kondo, A.; Nishimura, S.; Miyauchi, Y.; Nishii, Y.; Watanabe, K.; Takeuchi, H. *Colloid Surf., A* **2002**, *204*, 193.
(71) Lipgens, S.; Schubel, D.; Schlicht, L.; Spilgies, J.-H.; Ilgenfritz, G. *Langmuir* **1998**, *14*, 1041.
(72) Eisenberg, D.; Kauzmann, W. *The Structure and Properties of Water*; Clarendon Press: Oxford, U.K., 1969.
(73) Franks, F. *Water—A Comprehensive Treatise*; Plenum: New York, 1972.
(74) Nibbering, E. T. J.; Elsaesser, T. *Chem. Rev.* **2004**, *104*, 1887.
(75) Pimentel, G. C.; McClellan, A. L. *The Hydrogen Bond*; W. H. Freeman and Co.: San Francisco, CA, 1960.
(76) Lawrence, C. P.; Skinner, J. L. *J. Chem. Phys.* **2002**, *117*, 8847.
(77) Smith, J. D.; Saykally, R. J.; Geissler, P. L. *J. Am. Chem. Soc.* **2007**, *129*, 13847.
(78) Mukamel, S. *Annu. Rev. Phys. Chem.* **2000**, *51*, 691.
(79) Mukamel, S. *Principles of Nonlinear Optical Spectroscopy*; Oxford University Press: New York, 1995.
(80) Kwak, K.; Park, S.; Finkelstein, I. J.; Fayer, M. D. *J. Chem. Phys.* **2007**, *127*, 1245031.
(81) Roberts, S. T.; Loparo, J. J.; Tokmakoff, A. *J. Chem. Phys.* **2006**, *125*, 084502.
(82) Schmidt, J. R.; Roberts, S. T.; Loparo, J. J.; Tokmakoff, A.; Fayer, M. D.; Skinner, J. L. *Chem. Phys.* **2007**, *341*, 143.
(83) Steinel, T.; Asbury, J. B.; Corcelli, S. A.; Lawrence, C. P.; Skinner, J. L.; Fayer, M. D. *Chem. Phys. Lett.* **2004**, *386*, 295.
(84) Raugei, S.; Klein, M. L. *J. Chem. Phys* **2002**, *116*, 196.
(85) Nigro, B.; Re, S.; Laage, D.; Rey, R.; Hynes, J. T. *J. Phys. Chem. A* **2006**, *110*, 11237.
(86) Guardia, E.; Laria, D.; Marti, J. *J. Phys. Chem. B* **2006**, *110*, 6332.
(87) Chowdhuri, S.; Chandra, A. *J. Phys. Chem. B* **2006**, *110*, 9674.
(88) Dokter, A. M.; Woutersen, S.; Bakker, H. J. *Phys. Rev. Lett.* **2005**, *94*, 178301.
(89) Harpham, M. R.; Ladanyi, B. M.; Levinger, N. E.; Herwig, K. W. *J. Chem. Phys.* **2004**, *121*, 7855.
(90) Lipari, G.; Szabo, A. *J. Am. Chem. Soc.* **1982**, *104*, 4546.
(91) Laage, D.; Hynes, J. T. *Proc. Nat. Acad. Sci., U.S.A.* **2007**, *104*, 11167.
(92) Seifert, G.; Patzlaff, T.; Graener, H. *Phys. Rev. Lett.* **2002**, *88*, 147402.
(93) Faeder, J.; Ladanyi, B. M. *J. Phys. Chem. B* **2000**, *104*, 1033.
(94) Abel, S.; Sterpone, F.; Bandyopadhyay, S.; Marchi, M. *J. Phys. Chem. B* **2004**, *108*, 19458.
(95) Theodorou, G.; Rice, T. M. *Phys. Rev. B* **1978**, *18*, 2840.
(96) Lipgens, S.; Schubel, D.; Schlicht, L.; Spilgies, J.-H.; Ilgenfritz, G.; Eastoe, J.; Heenan, R. K. *Langmuir* **1998**, *14*, 1041.
(97) Abel, S.; Waks, M.; Marchi, M.; Urbach, W. *Langmuir* **2006**, *22*, 9112.
(98) Spry, D. B.; Goun, A.; Glusac, K.; Moilanen, D. E.; Childs, W.; Fayer, M. D. *J. Am. Chem. Soc.* **2007**, *129*, 8122.
(99) Moilanen, D. E.; Spry, D. B.; Fayer, M. D. *Langmuir* **2008**, DOI: 10.102/la703358a.